Eur. Phys. J. D **54**, 643–655 (2009)
DOI: 10.1140/epjd/e2009-00189-2

THE EUROPEAN PHYSICAL JOURNAL D

Regular Article

Density functional study of the electronic structure and properties of lithium intercalated graphite

D. Bandyopadhyay[a]

Physics Group, Birla Institute of Technology and Sciences, Pilani, 333031 Rajasthan, India

Received 17 March 2008 / Received in final form 12 November 2008
Published online 30 June 2009 –

Abstract. Ab initio electronic-structure calculations are performed using density functional theory (DFT) with polarized basis set (LanL2DZ and 6-311G^{++}) within the spin polarized generalized gradient approximation for lithium intercalated graphite. Initially different benzene-Li^{+} model clusters are optimized on the basis of their total energy at room temperature. These model clusters are used to calculate the optimized structure of lithium intercalated graphite clusters. The resultant optimized structures are used to calculate dipole moment, ionization potential (IP), electron affinity (EA), binding energy (BE) and vibrational spectra (IR and Raman). For an idea of the band gap of the clusters in the ground state, the HOMO-LUMO gap (ΔE_g) has been calculated. To compare the electron transfer ability of different clusters, chemical potential (μ), hardness (η) and their ratio ($|\frac{\mu}{\eta}|$) for different clusters have also been determined.

PACS. 31.15.E- Density-functional theory – 32.10.Hq Ionization potentials, electron affinities – 36.20.Ng Vibrational and rotational structure, infrared and Raman spectra

1 Introduction

One of the main objectives of designing batteries is to find a combination of low weight anode and cathode materials yielding the highest potential and capacity at low cost [1]. Such batteries are important candidates for use in portable devices like laptop computers, cell-phones, etc., and due to their compact size, high energy density and light weight. Improved efficiency and shorter recharging times with a large number of cycles gives a long life to these batteries [2]. Different doping elements are used either in one or both electrodes in such batteries to improve the above characteristics. The doping elements may be in the form of ions or in the form of neutral atoms as a defect or incorporated in the lattice in these intercalation compounds [3,4]. Pure lithium metal can be used as a very good negative electrode with low potential and high energy density in comparison to most of the transition metal cathodes. But its high exothermic reactivity causes self-heating that makes it unsafe for use in batteries [5,6]. Lithium metal also produces dendrites and other undesirable solid products due to reaction with the electrolyte that severely affects the reversible recycling process [1,4]. On the other hand in lithium intercalated graphite compounds, the dominating element graphite is stable in all ambient atmospheres and does not need a special environment in production. It also provides the best compromise between specific capacity and reversible cycle processes [1]. The potential of lithium intercalated graphite is close to that of lithium metal and due to the low weight of graphite, it is an ideal replacement of lithium as the negative electrode. Moreover, lithium intercalated compounds increase the conductivity to a large extent due to the presence of graphite layers [1]. Therefore lithium intercalated graphite anodes are very prominent in rechargeable batteries. Different experimental research has been undertaken on lithium intercalate graphite systems to improve their potential profile during lithium interaction with graphite, and to relate it with the staging phenomenon [7,8]. The graphite lattice has great influence on the reversible lithium capacity as well as the decomposition process occurring during lithium intercalation. Since the microstructure of the lattice plays an important role in these processes, computational quantum chemistry techniques have been applied to investigate the microstructure and properties of lithium intercalated systems. A number of theoretical studies have been reported on this system [9–11]. Although the composition ratio of the lithium present in the graphite lattice is generally taken as the rather stable configuration of LiC_6, it is important to examine the stability of other configurations to find an alternative, since incorporating more lithium atoms/ions in the lattice leads to an augmentation of the battery performance. In this study lithium atoms are systematically inserted into the graphite lattice. To obtain a realistic picture of lithium intercalated graphite, different model clusters based on benzene rings are used. In case of model structures, the edge distortion of the graphite layers is found to be minimal. So, the prime focus of the investigation is to study the structures and properties of the small Li-graphite or Li^{+}-graphite clusters based on total energy of the cluster in aromatic molecular form. Also it

[a] e-mail: rajuban@gmail.com; bandy@bits-pilani.ac.in

is important to investigate how the bigger molecules can absorb the lithium atom/atoms in the intercalated system in the form of small Li^+-graphite clusters of different sizes. Different combinations of benzene rings and larger polyaromatic hydrocarbons (bisbenzene, anthracene, etc.) are used as a model before applying the results to Li intercalated graphite. Hydrogen atoms are used with the different sized graphite sheets to terminate the unsaturated carbon bonds. This method is basically extending finite size graphite planes into larger planes. This also reduces the edge distortion when the planes interact with the lithium ions and also the optimization time. In the present calculations two different kinds of structures are used. In the first, different clusters with neutral lithium atom/atoms between the graphite planes of different sizes are taken. Next, their ionized structures, both in cationic and anionic states, have been studied. In the next series of structures, hydrogen terminated graphite planes of different sizes have been studied after adding lithium ion(s). This second category of structures is close to lithium bonding with the graphite lattice. It is known that neutral lithium atoms in the gas phase (Li^0) reacts with aromatic compounds such as benzene or anthracene, yielding a product which is either a lithium atom aromatic compound adduct or a lithium-ion aromatic molecule anion radical (AR). Therefore the above mentioned structures have been chosen for calculation. Multiple starting structures have been optimized to find the lowest energy isotope. The ground state optimized structures have been used to determine geometrical parameters (such as bond length, bond angle, etc.), ionization potential, electron affinity, binding energy per atom in the cluster, HOMO-LUMO gap, electronic charge distributions in the highest and lowest filled orbitals. Finally to aid identification, infrared and Raman frequencies and intensities have also been calculated for selected clusters.

2 Methodology

The present calculations are performed using a density functional theory (DFT) with spin polarized generalized gradient approximation (GGA) using the Perdew-Wang exchange and Perdew-Wang 91 correlation [12–16] techniques for all clusters. Self-consistent-field (SCF) electronic structure calculations are carried out on all clusters. Two different basis sets (LanL2DZ and 6-311G^{++}) are used in the present calculations. For optimization of all model clusters with hydrogen termination LanL2DZ as well as 6-311G^{++} basis was used and for the lithium intercalated graphite clusters a 6-311G^{++} basis was used. The LanL2DZ basis set is very effective as a core potential with no symmetry constraints [17–20]. The optimized electronic structure is obtained by solving the Kohn–Sham equations self-consistently. Geometry optimizations were carried out with a convergence limit of 10^{-7} hartree on the total energy. Structures were relaxed using the conjugate gradient method for different fixed spin multiplicities and with no symmetry constraints. Electronic properties were calculated from the SCF total electronic energy and the orbital energy values. All theoretical calculations are performed with the GAUSSIAN-98 program package [21]. The optimization of the structures is confirmed by checking harmonic vibrational frequency calculations (IR and Raman). If an imaginary vibrational mode is found, a relaxation along the coordinates of this mode is carried out until the true local minimum is actually obtained.

3 Results and discussions

In the present calculations combinations of Li ions with graphite layers (pure and hydrogen terminated) are taken in the form of small clusters, where the carbon atoms are treated as part of a graphite layer. Therefore different hexagonal carbon rings in the present calculation appear as different graphite planes in combination with Li^+. The following optimized structures have been fully optimised; benzene, benzene-Li^+, benzene-2Li^+, 2(benzene)-Li^+, 2(benzene-Li^+), 3(benzene)-2Li^+, 4(benzene)-2Li^+, anthracene-benzene-Li^+, bis(anthracene-AR-Li^+), 2($C_{16}H_{16}$-Li^+) and 2($C_{24}H_{12}$)-Li^+. The benzene rings are then replaced by finite graphite planes without the presence of hydrogen. In such calculation it has been found that since graphite planes are much bigger than the sphere of influence of a single or pair of Li^+ ions, in most cases for relatively larger clusters the edge carbon atoms in the graphite layers are not affected due to the interaction with the Li^+ ions, except the change in inter-planar distance between different graphite layers. It is also found that the geometry of the benzene rings in the graphite layers remains the same even with the presence of Li^+ ion/ions near or in-between the graphite layers. To check the validity of using the above model clusters, several thermodynamic parameters of the model clusters are calculated and presented in Table 1. These parameters are very close to values reported previously [22].

Different optimized model clusters (i.e. Li^+-graphite planes with hydrogen termination) calculated using 6-311G^{++} and LanL2DZ basis sets are shown in Figure 1. The calculated clusters using different methods are almost identical except small changes in the structural parameters. Parameters obtained by the two methods are shown in Table 2. As the first member of the present series, a benzene ring is first studied. Its average C–C and C–H bond lengths are 1.40 Å and 1.09 Å respectively. Average bond angles between successive carbon atoms in the benzene ring are 120.0°. Both parameters are very close to experimental values. Other parameters of the cluster are shown in Table 2. Addition of a lithium ion with the carbon ring in the benzene gives benzene-Li^+ cluster and its optimized structure is shown in Figure 1. This is like a hexagonal capped pyramid structure where the benzene ring is a part of a graphite basal plane. Addition of the Li^+ ion increases the size of the benzene ring. The average bond length between the carbon atoms in the benzene ring in the optimized cluster is 1.41 Å. The average distance between the lithium and carbon atoms is

Table 1. Different thermodynamic parameter of the model clusters.

Clusters	E_{Thermal} (kCal/mol)	$E_{\text{Zero Point}}$ (kCal/mol)	S_{Entropy} (kCal/mol Kelvin)	C_v (kCal/mol kelvin)
benzene	67.03	64.33	68.84	16.66
benzene-Li^+	69.30	65.73	74.44	21.73
benzene-2Li^+	70.76	65.24	94.60	28.09
2(benzene)-Li^+	138.52	131.06	110.89	43.97
2(benzene-Li^+)	139.51	130.40	132.03	49.94
anthracene-benzene-Li^+	201.04	190.95	129.96	64.91
3(benzene)-2Li^+	206.53	196.43	138.22	61.98
bis(anthracene-AR-Li^+)	267.07	252.54	165.46	93.19

E_{Thermal}: thermal energy of the cluster; $E_{\text{Zero Point}}$: zero point energy of the cluster; S_{Entropy}: total molar entropy of the cluster; C_v: specific molar heat capacity of the cluster.

Table 2. Dipole moment, band gap and average binding energy per atom of different lithium-carbide clusters.

Clusters	Moment (debye)		ΔE_g (eV)		BE per atom (eV)	
	LanL2DZ	$311G^{++}$	LanL2DZ	$311G^{++}$	LanL2DZ	$311G^{++}$
benzene	0.33	0.33	7.13	7.13	7.04	7.04
benzene-Li^+	5.38	5.05	7.32	7.38	6.61	6.67
benzene-2Li^+	0.00	0.00	6.67	6.78	5.97	5.94
2(benzene)-Li^+	0.02	0.03	6.75	6.78	6.86	6.92
2(benzene-Li^+)	0.01	0.04	6.30	6.40	6.50	6.47
anthracene-benzene-Li^+	3.00	3.11	3.86	3.92	7.41	7.37
3(benzene)-2Li^+	0.08	0.08	5.96	6.12	6.72	6.70
bis(anthracene-AR-Li^+)	0.00	0.00	3.46	3.48	7.52	7.50
2(C16H10-Li^+)	0.03	0.04	3.78	3.84	7.83	7.80
2(C24H12)Li^+	0.08	0.08	4.11	4.14	8.49	8.45

2.4 Å. The bond length between the carbon and hydrogen decreases from 1.09 Å to 1.08 Å. Due to the presence of the lithium ion the cluster has a large electric dipole moment of 5.38 debye. The charge carried by each carbon atom −0.24e, which is −0.23e in the benzene ring. The charge carried by the hydrogen atoms are changes from 0.23e to 0.30e from benzene to benzene-Li^+ cluster. Since the excess positive charge is shared among the atoms in benzene-Li^+ cluster, the size of the benzene ring expands. The total positive charge of the Li^+ ion is 0.70e. The calculated HOMO (highest occupied molecular orbital) of this cluster is slightly different from that of the benzene ring and it extends up to the surrounding region of the lithium ion symmetrically as shown in Figure 2. Like the HOMO, the LUMO (lowest unoccupied molecular orbital) in the benzene-Li^+ cluster is also extended near Li^+ as shown in Figure 2. The HOMO-LUMO gap obtained by the LanL2DZ method is 7.32 eV. Compared to the benzene-Li^+ cluster, a C_6-Li^+ cluster obtained using a 6-$311G^{++}$ basis is different. In this cluster all the atoms are positively charged. The HOMO is mostly symmetrical about the graphite plane. Similarly, the LUMO is also symmetrical about the graphite plane and the Li^+ ion is not holding any LUMO. As for the benzene-Li^+ cluster, the Li^+ ion also shows no HOMO character close to it. The shape of both these orbitals is different from the benzene-Li^+ cluster. Here the HOMO-LUMO gap is 2.83 eV which is much lower than the benzene-Li^+ cluster. Therefore in small size $C_mLi_n^+$ clusters are more favourable than benzene-Li^+ clusters for conduction of electrical charge. Calculated stabilities show that both the clusters are not stable and the binding energy per atom in benzene-Li^+ is more than C_6Li^+ cluster. Therefore the presence of the hydrogen makes the small cluster more stable due to proper balancing of strain acting between the C–C bonds in a hexagonal carbon ring which is a part of graphite plane.

Addition of one more Li^+ ion to the benzene-Li^+ optimized structure gives benzene-2Li^+ cluster. Though the initial guess geometry of this structure is symmetrical where the Li^+ ions are placed symmetrically on both sides of the benzene ring, the optimized structure is no longer symmetrical. The two lithium ions divert from the axial position of the benzene ring to lie at the diametrical position and above the benzene plane. The separation between the lithium ions in the optimized structure is 6.03 Å, whereas the bond length between the nearest carbon atom of the benzene ring and the lithium ion is 2.54 Å on both sides. The angle formed by the lithium atom, nearest carbon and farthest carbon atom in the benzene ring is 95.4°. This distorted structure is due to the excess amount of positive charges present in the cluster. Two different bond

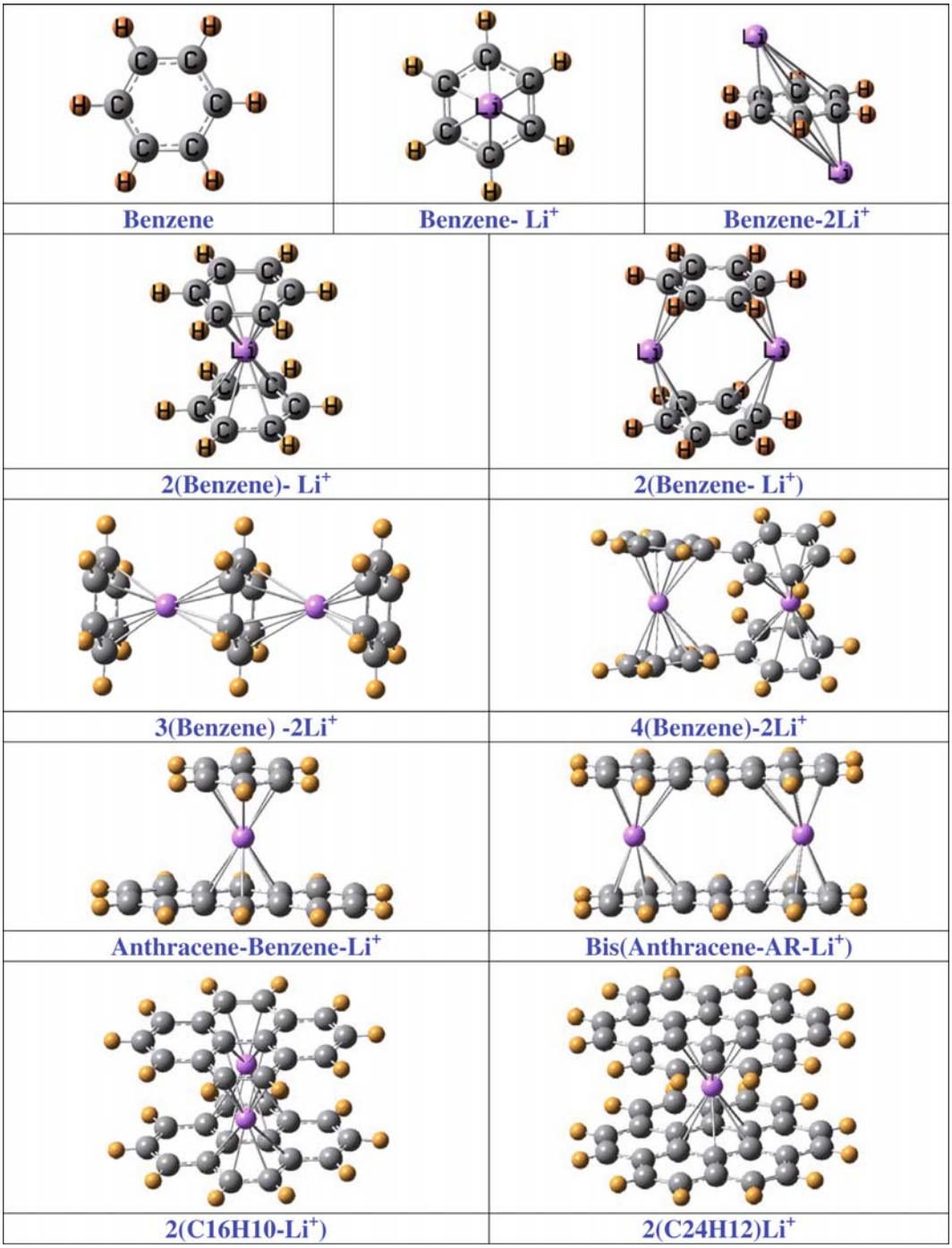

Fig. 1. (Color online) Different optimized model clusters.

lengths between the carbon atoms are present in the benzene ring and are 1.41 Å and 1.414 Å. In the cluster, charge carried by each atom is distributed symmetrically. The charge distribution in the carbon atoms in the benzene ring is not uniform. The lithium atoms carry the same amount of +0.91e charge. The two nearest carbon atoms to the lithium atoms carry the same amount of negative charge −0.41e. The other four carbon atoms carry ± 0.24e. Although this is an asymmetrical structure, the HOMO orbital distribution is symmetrical about the benzene plane, whereas the LUMO orbitals extend up to the position of lithium atoms on both sides. The charge in the cluster distributes among the atoms in such a manner that the whole cluster has a very low electric dipole moment. The HOMO-LUMO gap of the cluster is 6.66 eV, which is lower than the benzene-Li^+ cluster. Its binding energy is also lower that the benzene-Li^+ cluster as shown in Table 2. Compared to benzene-$2Li^+$ the C_6-$2Li^+$ cluster has lower HOMO-LUMO gap as well as lower binding energy per atom. Its charge distribution is also different

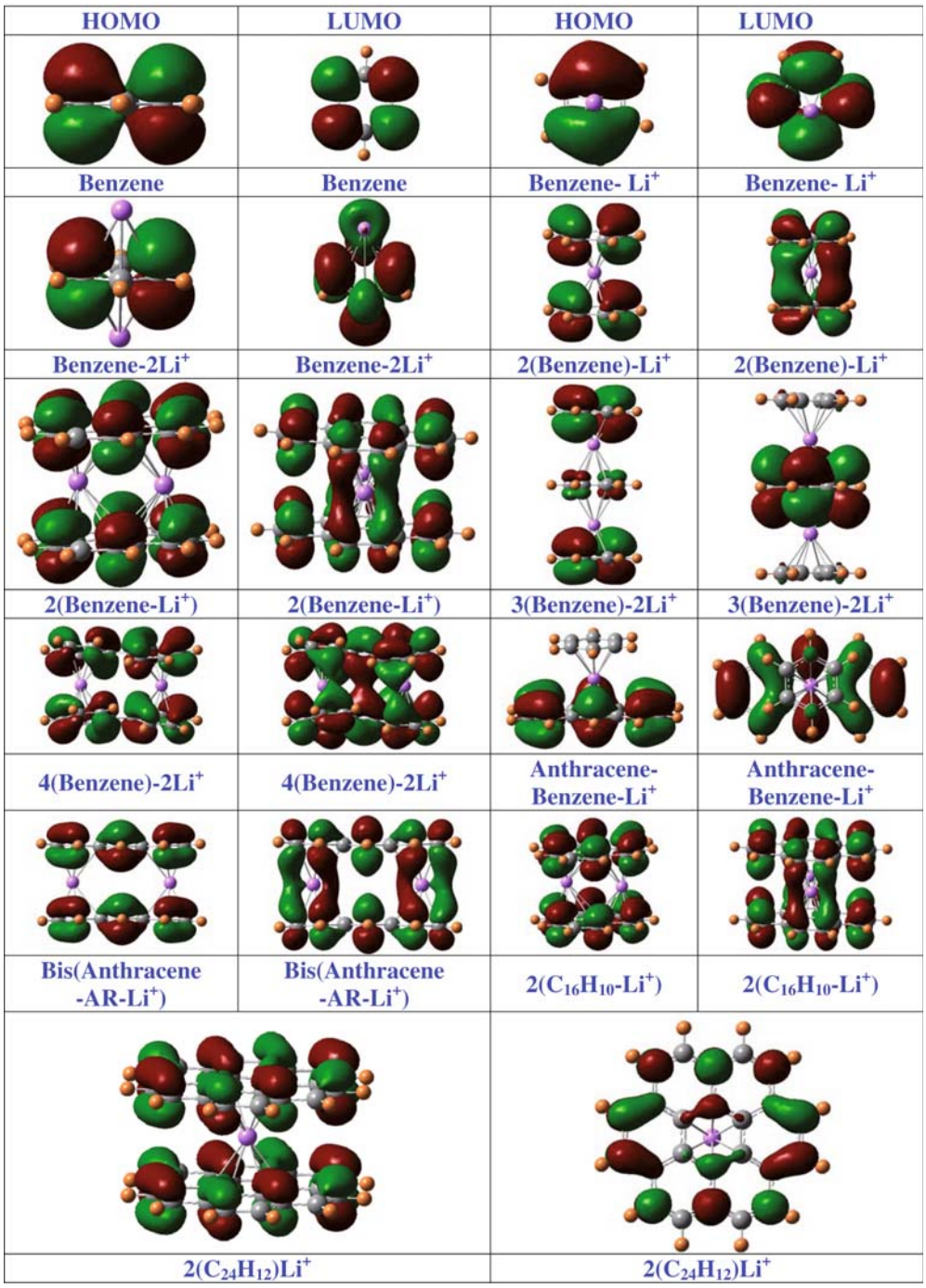

Fig. 2. (Color online) HOMO-LUMO distributions of Li^+ intercalated graphite (with hydrogen terminated) system by using LanL2DZ and 6-311G^{++} basis set.

from benzene-2Li$^+$ cluster and follows the same nature as the C_6-Li$^+$ cluster discussed before. The HOMO is distributed both in the inner and outer region of the plane of the hexagonal carbon ring and the distribution is well away from the position of the lithium atoms. The LUMO orbital distribution is mainly extended on the outer region of the carbon ring, keeping the inner region and the surrounding region of the lithium atoms empty.

Addition of one benzene ring to the benzene-Li$^+$ cluster forms a symmetrical 2(benzene)-Li$^+$ cluster as a small model structure of lithium ion between two graphite planes. The optimized structures obtained by 6-311G^{++} and Lan2DZ basis show that both benzene planes are parallel and symmetrically placed about the lithium ion. The average bond length between the carbon atoms in the benzene rings in the optimized cluster reduces from 1.42 Å in

benzene-Li^+ cluster to 1.41 Å and the C–H remains unchanged at 1.08 Å. Therefore the carbon ring in the benzene structure reduces in the 2(benzene)-Li^+ cluster. The charge carried by each carbon atoms in this cluster is the same but smaller than that of the benzene-Li^+ cluster. This is true for hydrogen atoms also. The carbon atoms charge change from −0.24e to −0.22e from benzene-Li^+ to 2(benzene)-Li^+, whereas the hydrogen charge changes from 0.30e to 0.28e. In comparison to the change of the amount of charge carried by carbon and hydrogen in 2(benzene)-Li^+ cluster, the change is more in the case of the Li atom in the 2(benzene)Li^+ cluster. The charge carried by lithium in 2(benzene)-Li^+ cluster is 0.32e which is much lower than the same carried by Li in the benzene-Li^+ cluster. This is due to the sharing of same amount of unit positive charge between all atoms in the small cluster. The HOMOs and LUMOs are show in Figure 2. The HOMOs are symmetrically distributed about the benzene planes with resultant dipole moment of the cluster 0.02 debye. On the other hand, the LUMOs are extended surrounding to the lithium between the regions of the two benzene planes as shown. The HOMO-LUMO gap of this cluster (6.75 eV) is lower than the benzene-Li^+ cluster (7.32 eV). Its binding energy per atom is relatively higher than that of the previously discussed clusters. Removal of hydrogen from 2(benzene)Li^+ cluster forms a small cluster of lithium intercalated graphite system where the lithium atom can be found symmetrically between the two graphite hexagonal rings. Its binding energy per atom is higher than that of the C_6Li^+ and C_6-$2Li^+$ clusters, but the HOMO-LUMO gap is lower than in both of these clusters. The HOMO orbital distribution in the graphite rings is diagonally symmetrical in the cluster. Like other carbon rings, the HOMO, distributed in the hexagonal carbon plane only keeps the lithium atom's region empty, whereas the LUMO in C_6Li^+ cluster is as shown in Figure 3. Different parameters related to these clusters are shown in Table 3.

Addition of one more lithium ion between the region of two benzene rings can form the optimized 2(benzene-Li^+) cluster as shown in Figure 1. Like benzene-$2Li^+$ cluster, here also the bond lengths between the carbon atoms in benzene rings are of two types, 1.41 Å and 1.413 Å. The distance between the lithium atoms is 3.90 Å, whereas the bond length between the lithium and nearest carbon in the benzene ring is 2.34 Å. The angle between the lithium, nearest and farthest carbon atom in the benzene ring is 103.24°. This is higher than the same angle in the benzene-$2Li^+$ cluster. The lithium atoms in the cluster carrying an average charge 0.69e, whereas the carbon and hydrogen atoms are negative and positive respectively. Its HOMO-LUMO gap as well as the binding energy per atom is less than the 2(benzene)-Li^+ cluster. The reduced binding energy could be due to the excess ratio of the carbon to lithium atoms in the cluster and also due to its charged nature. Orbital charge distributions also follow the same trend as the smaller clusters. The HOMO is only distributed about the plane of the benzene ring and there is no extension of the orbitals surrounding the lithium atom. On the other hand, the LUMO surrounds the lithium atoms and distributed about the benzene ring planes. It is to be noted that in all HOMOs, the charge distributions are symmetrical about the benzene planes, but with opposite charge sign. This is also true for the two parallel benzene planes when compared their HOMO orbital distributions. For the LUMO, about the benzene plane, the orbital charge distributions have opposite signs, but this is the same between two parallel benzene rings. Therefore in the presence of the lithium ion between the parallel benzene rings, the LUMOs in the region between the planes overlap and hence surround the lithium atom. The graphite-Li^+ clusters do not show any of this behaviour. In this cluster the HOMO charge distributions are only in the graphite planes and the LUMO is about the planes. But the lithium ions are always far from any of the orbital charge distributions. The interesting point in this cluster is the charge carried by each atom. Both carbon and lithium ions are positive in this cluster. The HOMO-LUMO gap and the binding energy per atom in this cluster are 2.6 eV and 5.63 eV. Both of these values are smaller than the 2(benzene-Li^+) cluster as shown in Table 2.

The HOMO-LUMO distribution of 3(benzene)-$2Li^+$ is very symmetrical and is shown in Figure 2. The HOMO orbital charge distribution about the middle benzene plane is much smaller than the other two parallel planes. This is just opposite in LUMO orbital distribution. Here most of the distribution is about the middle planes whereas the other two planes are almost completely empty. In the same kind of graphite-$2Li^+$ cluster, the HOMO can be found only about the one outer carbon ring, but the LUMO is distributed only about the middle carbon ring. In this cluster the HOMO-LUMO gap is much smaller than the 3(benzene)-$2Li^+$ cluster, but the binding energy is close to it. Other structural parameters of this cluster are the same as the benzene-Li cluster. The nature of charges carried by the carbon and the lithium atoms is just opposite to that in the benzene-Li^+ cluster. All carbon atoms in the outer two rings carry an average 0.142e, whereas the carbon atoms in the middle section carry an average of 0.165e. The negative charge carried by each benzene atom is −0.34e. Average positive charge carried by the lithium ions is 0.45e whereas all carbon atoms are negatively charged. The average charges carried by the carbon atoms in the two outer benzene rings are both −0.23e, the connected hydrogen atoms are all positive and carrying 0.29e amount of positive charge. The carbon atoms in the middle benzene ring are carrying relatively higher amount of negative charge −0.26e. Due to addition of lithium ions or the benzene rings, there is redistribution of charge in the atomic sites, but the change in bond length between the carbon atoms is negligible. In the present cluster the bond length between the carbon atoms in the benzene ring varies from 1.41 Å to 1.42 Å. The HOMO-LUMO gap and the binding energy per atom in this cluster are 5.96 eV and 6.72 eV respectively.

The next model structure to study the extended graphite-Li^+ system is anthracene-benzene-Li^+ as shown in Figure 1. The lithium ion is at the middle position of

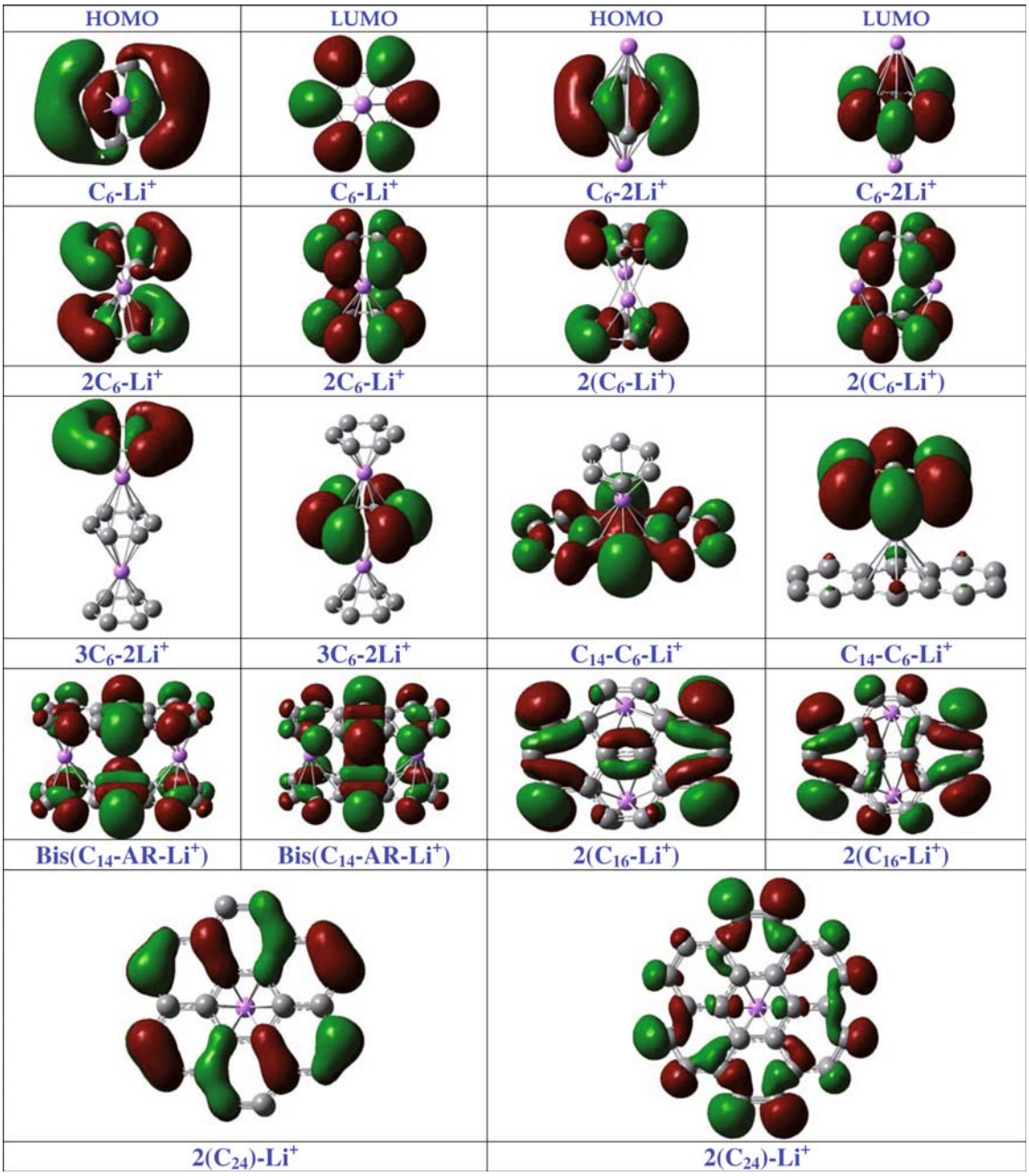

Fig. 3. (Color online) HOMO-LUMO distributions of Li^+ intercalated graphite system by using 6-311G^{++} basis set.

Table 3. Dipole moment, band gap and average binding energy per atom, etc. of different lithium-carbide clusters.

Clusters	Moment (debye)	ΔE_g (eV)	BE per atom (eV)	Charge on Li in the cluster (e)
C_6-Li^+	5.75	2.83	5.84	0.67
C_6-$2Li^+$	0.00	2.69	4.80	0.81
$2(C_6)$-Li^+	0.00	2.78	6.29	0.32
$2(C_6$-$Li^+)$	0.00	2.60	5.63	0.52
C_{14}-C_6-Li^+	0.17	1.50	6.00	0.34
$3(C_6)$-$2Li^+$	0.91	0.95	6.82	0.43
bis(C_{14}-AR-Li^+)	0.07	0.76	6.74	0.52
$2(C_{16}$-$Li^+)$	0.01	0.65	7.05	0.76
$2(C_{24})$-Li^+	0.07	2.61	7.81	0.89

the two central benzene rings and the bond lengths between the carbon atoms and the benzene rings vary from 2.43 Å to 2.46 Å, whereas the bond length between successive carbon atoms in the benzene rings varies from 1.20 Å to 1.45 Å. The lithium atom is carrying 0.34e amount of charge, whereas all carbon atoms are negatively charged. It is interesting to watch the HOMO orbital distribution in this cluster. All distribution is about the extended planes containing three benzene rings. There is no distribution surrounding the single benzene ring on the other plane and also around the lithium ion. The top view of LUMO charge distribution of this cluster is shown in Figure 2. Here the LUMO distributions are extended between pairs of carbon atoms in the bigger plane in the cluster. In both the case the lithium atom is not surrounded by the orbital distributions. Therefore in this cluster the LUMO orbital distribution is not between the two planes, it is only in the extended plane. The HOMO-LUMO gap in this cluster is relatively lower than other cluster of value 3.86 eV, but the binding energy per atom is 7.40 eV. The optimized structure of the same kind graphite-Li^+ system is same as the anthracene-benzene-Li^+ system, but its HOMOs-LUMOs are completely different from anthracene-benzene-Li^+ as shown in Figure 3. The HOMO is distributed about the extended graphite planes, but LUMO can be found only in the region about the smaller graphite plane. In this cluster the HOMO-LUMO gap (= 0.95 eV) is lower then the previous graphite-Li^+ clusters, but binding energy per atom (= 6.82 eV) is much higher. In graphite-Li^+ system, the binding energy is almost comparable to the same kind of benzene-Li^+ system. In other bigger clusters, both HOMO and LUMO are symmetrically distributed in the two parallel planes keeping the lithium ion with an empty region surrounding of it. HOMO-LUMO gap in both the model as well as in lithium intercalated graphite clusters decreases with the increase of the size of the clusters. In intercalated clusters, the HOMO-LUMO gap is minimum for $2C_{24}$-Li^+ cluster as shown in Figure 5. The binding energy of all clusters has a tendency to increase with the size of the clusters. The binding energies obtained using LanL2DZ and 6-311G^{++} basis sets are comparable to each other in the model clusters, but are different from that obtained in the intercalated graphite-Li^+ system.

3.1 Study of binding energy (BE), HOMO-LUMO gap (ΔE_g), charge on Li atom and vibrational spectra of the clusters

Variation of binding energy of the model clusters as well as the lithium intercalated graphite clusters are shown in Figure 4. From the figure it is clear that with increasing cluster size, keeping the benzene rings as parallel planes, the binding energy both in the model clusters and in the lithium-graphite clusters increases. It is interesting to note that in the same size of graphite or benzene planes (in model clusters), addition of more lithium atoms decreases the binding energy. This is due to the repulsive forces between two lithium atoms in the clusters carrying positive charge. With the increase of separation between the

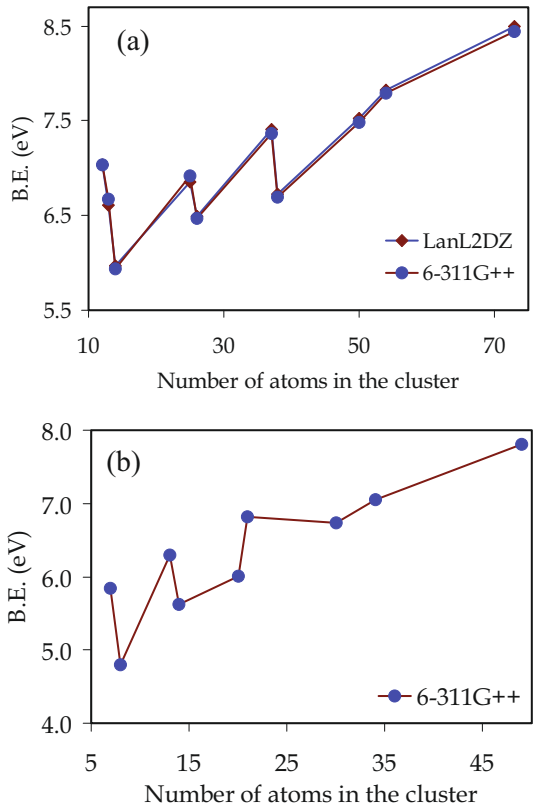

Fig. 4. (Color online) Variation of binding energies of different clusters with the number of atoms in it: (a) model clusters, (b) lithium intercalated graphite clusters.

lithium atoms in relatively bigger clusters, the binding energy of the clusters increases because of reduced repulsion between the lithium atoms. Binding energy per atom in the model clusters is higher than that of the lithium graphite system. This is because of strong bonding nature between the carbon and hydrogen atoms in the benzene rings. Both the binding energy graphs show that the variation of B.E.'s is regular and increases with the size of the cluster. Figure 4 also shows that in case of symmetrical clusters, like, 2(benzene)-Li^+; 3(benzene)-Li^+, 2(C_6)-Li^+, 3(C_6)-2Li^+ and in the bigger clusters where the separation between the Li^+ atoms are higher, the binding energy per atom is also high. So both the structure as well as the size of the cluster is responsible for higher binding energy of the clusters.

The variation of HOMO-LUMO gap also follows the same trend both in model clusters and in lithium intercalated graphite clusters and is shown in Figure 5. With the increase of the size of the clusters, the HOMO-LUMO gap decreases. In the model clusters, a sudden jump in the gap is due to instability because of the presence of more number of lithium atoms in a small cluster. This is absent in the lithium graphite system. The nature of the variation of both the HOMO-LUMO graph (Fig. 5) with the number of the atoms in the clusters indicates that the conductivity of the clusters increases with the size of the cluster in a symmetric manner.

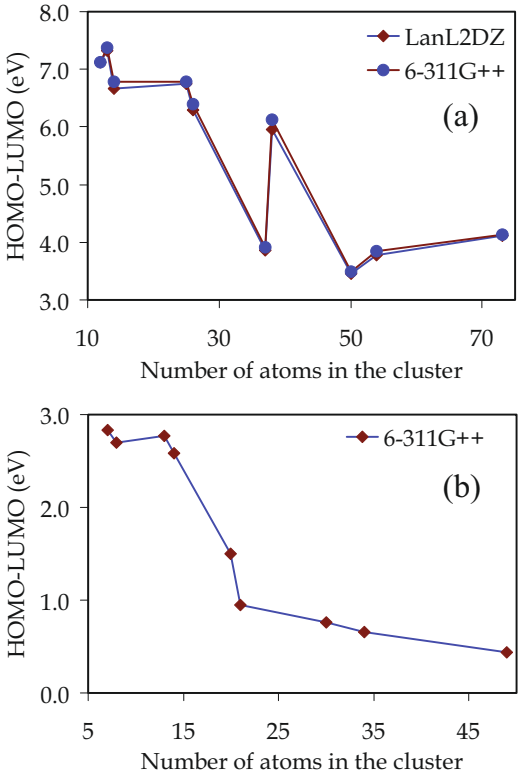

Fig. 5. (Color online) Variation of HOMO-LUMO gap of different clusters with the number of atoms in it: (a) model clusters, (b) lithium intercalated graphite clusters.

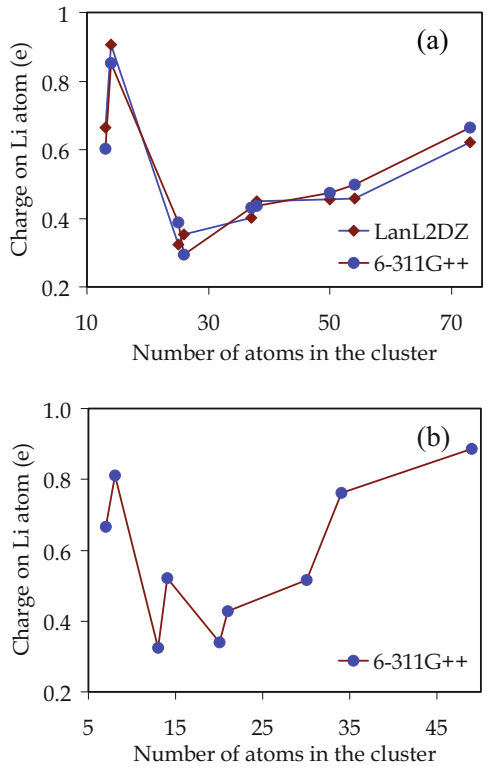

Fig. 6. (Color online) Variation of charge on the lithium atoms in different clusters with the number of atoms in it: (a) model clusters, (b) lithium intercalated graphite clusters.

Variation of the amount of charge carried by the lithium in the clusters with the number of the atoms present in the clusters is shown in Figure 6. With the increase of the cluster size, the charge carried by the lithium atoms decreases and then increases in bigger clusters. The bigger clusters are symmetric, relatively stable and have higher binding energy. Therefore, the large graphite planes with intercalated lithium atoms can be taken as the better medium for charge conduction.

In order to check the dynamical stability of the clusters vibrational spectra of the model clusters are studied and presented in Figure 7. In most of the clusters the spectra shows sharp peaks without any presence of imaginary frequency. Sharp peaks in the spectrum reflect the limited number of vibrational states in the cluster with better stability. The main difference between the most dominant frequencies in IR and Raman spectra are the mode of vibration. In IR the atoms in the clusters vibrate in different phases and this is true for all possible modes of vibrations, whereas in Raman there are two modes of vibrations where all atoms in the clusters vibrates in phase which looks like high symmetric breathing mode of the clusters. There is no existence of any imaginary frequencies in IR and Raman spectrum of the clusters, showing these clusters are all stable.

3.2 Ionization potential (IP), electron affinity (EA), chemical potential (μ) and chemical hardness (η)

Study of the effects of charging of the clusters is important in order to understand the electron affinity (EA) and ionization potential (IP) of the clusters. To estimate the potential ability of lithium intercalated graphite, small clusters of the system are taken as the charge sources to macroscopic bodies. This may be a first-step study to calculate their IP's and EA's. In the present work the energies of the anion and neutral clusters are also calculated to obtain both the EA's and IP's. Variations of EA's and IP's of clusters are shown in Figure 8. It is clear from the graph that there is not much variation of ionization potential and electron affinities with the number of the atoms in the cluster. Variation of these two parameters with the size of the clusters is opposite, though the variations are small. The rate of decrease of the ionization potential is slightly higher than the variation of electron affinities. Increase of electron affinities with the cluster size is a clear indication of increasing conductivity. This can be clearly understood from HOMO-LUMO charge distributions in the clusters as shown in Figure 3. In most of the clusters, added Li atom does not carrying any orbital charge distributions.

In practice, the chemical potential (μ) and chemical hardness (η) can be expressed in terms of ionization potential and electron affinity. It can also be expressed in terms of total energy consideration. If the total energy of N electron system is $E(N)$, then the energy of a system

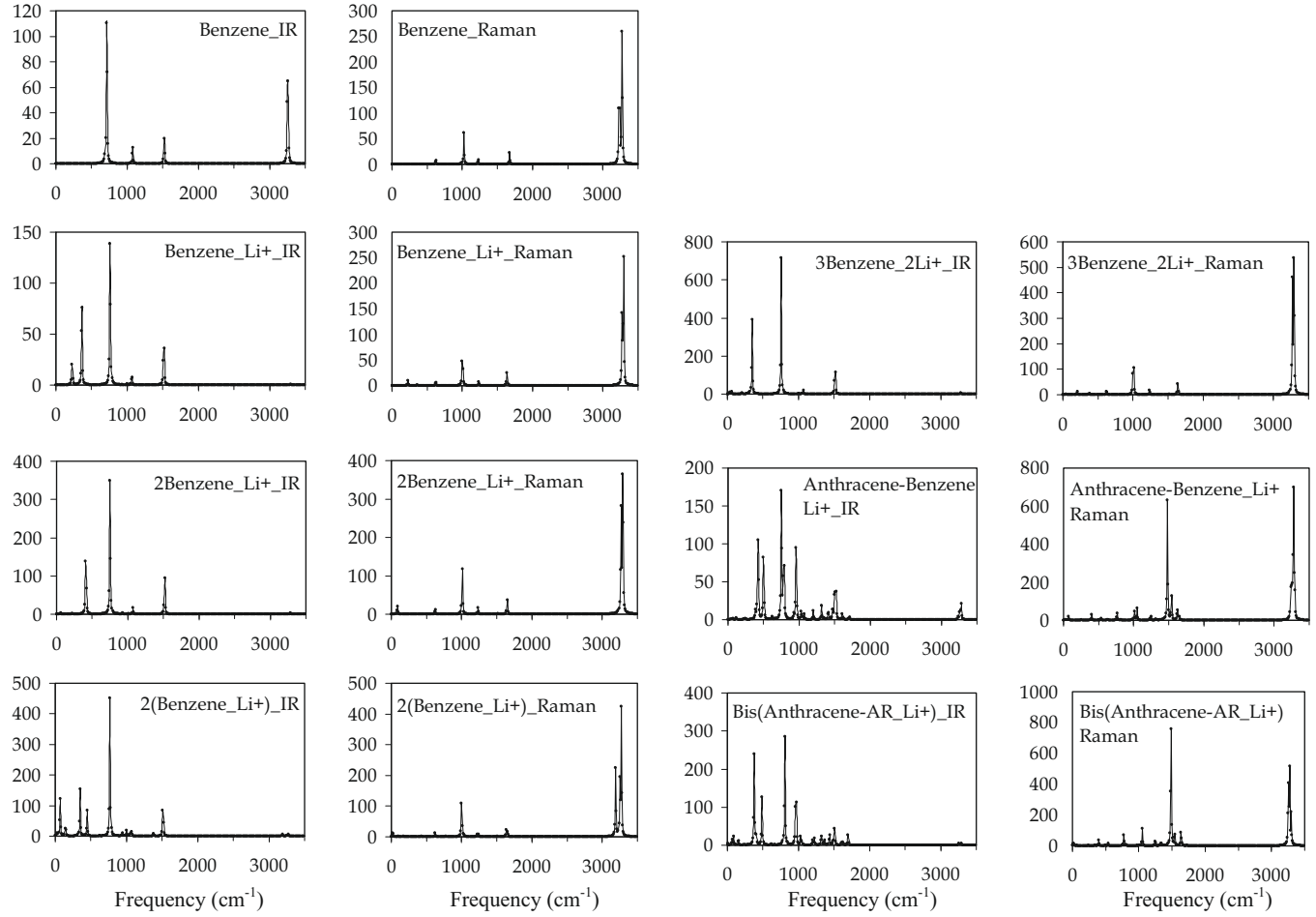

Fig. 7. IR and Raman spectrum of different model clusters obtained by using LanL2DZ/B3LYP method. The vertical axis representing the IR intensity of Raman activity.

containing $N+\Delta N$, where $\Delta N \ll N$ can be expressed as:

$$E\left(N+\Delta N\right) \simeq E\left(N\right) + \left.\frac{dE}{dx}\right|_{x=N} \Delta N + \frac{1}{2}\left.\frac{d^2E}{dx^2}\right|_{x=N} \left(\Delta N\right)^2.$$

Then μ and η are defined as

$$\mu \equiv \left.\frac{dE}{dx}\right|_{x=N} \quad \text{and} \quad \eta = \frac{1}{2}\left.\frac{d^2E}{dx^2}\right|_{x=N} = \frac{1}{2}\left.\frac{d\mu}{dx}\right|_{x=N}.$$

Since, $IP = E(N-1) - E(N)$ and $EA = E(N) - E(N+1)$, by setting $\Delta N = 1$, μ and η are related to IP and EA via

$$\mu = -\frac{IP+EA}{2} \quad \text{and} \quad \eta = \frac{IP-EA}{2}.$$

Consider two systems with μ_i and η_i $(i = 1, 2)$ contacting each other, where some amount of electron charge (ΔM) transfers from one to another. The quantity ΔM and the resultant energy change (ΔE) due to the charge transfer can be determined in the following way [23]. The total energies after charge transfer are

$$E_1\left(N_1+\Delta M\right) \simeq E_1\left(N_1\right) + \mu_1 \Delta M + \eta_1 \left(\Delta M\right)^2$$

and

$$E_2\left(N_2-\Delta M\right) \simeq E_2\left(N_2\right) - \mu_2 \Delta M + \eta_2 \left(\Delta M\right)^2.$$

Correspondingly, chemical potential become

$$\mu_1' = \left.\frac{dE_1\left(x+\Delta M\right)}{dx}\right|_{x=N_1} \simeq \mu_1 + 2\eta_1 \Delta M$$

and

$$\mu_2' = \left.\frac{dE_2\left(x-\Delta M\right)}{dx}\right|_{x=N_2} \simeq \mu_2 - 2\eta_2 \Delta M$$

to first order in ΔM after the charge transfer. Establishment of chemical equilibrium after charge transfer requires $\mu_1' = \mu_2'$ from which one can get,

$$\Delta M \simeq \frac{\mu_2 - \mu_1}{2\left(\eta_1+\eta_2\right)} \quad \text{and} \quad \Delta E \simeq \frac{\left(\mu_1-\mu_2\right)^2}{2\left(\eta_1+\eta_2\right)}.$$

In the above expression ΔE is the energy gain by the total system (1 and 2) due solely to the alignment of the

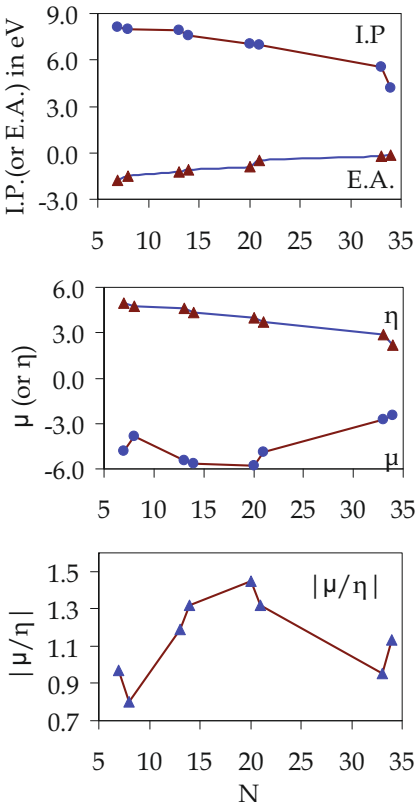

Fig. 8. (Color online) Variation of different parameters in lithium graphite system.

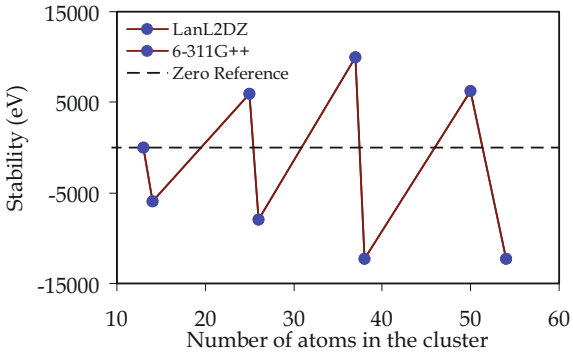

Fig. 9. (Color online) Variation of stability of the model clusters.

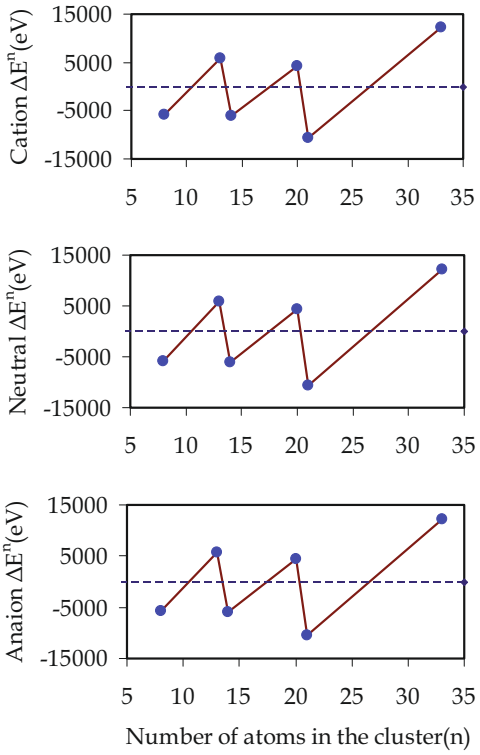

Fig. 10. (Color online) Variation of stability of lithium intercalated graphite system.

chemical potentials of the two systems at the same value. There may be an additional energy gain provided by Coulomb attraction between the two, if the initial states of both were charge neutral. It is evident from the expressions of ΔM and ΔE that a guiding principle to predict the occurrence of an easier charge transfer is a large difference in μ together with low η_1 and η_2.

Keeping the preliminaries above in mind, chemical potentials (μ) and chemical harnesses (η) for lithium intercalated graphite system have been calculated. For this purpose optimization of the clusters in neutral and ionized state with ± 1 charge have been done. To search for a cluster with a high ability to accept an electron with a low chemical hardness, $|\frac{\mu}{\eta}|$ ratios have been calculated and presented in Figure 8 along with the variation of μ and η with the number of atoms in the clusters. It shows that in the case of smaller cluster this parameter is higher than for the bigger clusters. Considering also the low chemical hardness (see expression of ΔM and ΔE), one can expect that the smaller clusters may serve as a charge-transfer-type acceptor to other substances, such as bigger graphite-Li clusters (or lattice) and this is also supported by the variation of the amount of charge carried by lithium atom in bigger clusters as shown in Figure 6.

In order to check the stabilities of the clusters, the successive variation in energy $[\Delta E^N = E(N+m) + E(N-n) - 2E(N)]$ for model clusters as well as in the intercalated neutral and charged clusters have been calculated. Stability plots of pure, cation and anion clusters are shown in Figures 9 and 10. Different parameters, such as like, IP, EA and stabilities of the charged clusters are given in Tables 4a and 4b. All stability plots are almost of the same kind except small variation in stability value. The clusters appearing with magic nature in the neutral state remains magic in nature in the model as well as in the lithium graphite system in different charged states. This shows the regular nature in stability of the clusters. In each group (i.e. same charge state) there is almost no variation in stability but when compared with other groups, a wide variation can be found from the data presented in Table 4.

Table 4a. Dipole moment, ΔE_g and binding energy per atom of lithium-carbide clusters in different charged states.

Clusters	Moment (debye)	ΔE_g (eV)	BE/atom (eV)	Clusters	Moment (debye)	ΔE_g (eV)	BE/atom (eV)
C_6-Li	5.22	2.58	6.19	$3C_6$-2Li	0.01	0.62	6.41
C_6-Li^+	5.75	2.83	4.80	$3C_6$-2Li^+	0.91	0.95	6.82
C_6-Li^-	4.77	1.51	6.38	$3C_6$-2Li^-	0.21	0.92	6.64
C_6-2Li	0.05	2.71	5.71	C_{14}-C_6-Li	0.25	0.76	6.97
C_6-2Li^+	0.00	2.69	4.84	C_{14}-C_6-Li^+	0.16	1.50	6.00
C_6-2Li^-	0.25	0.85	5.78	C_{14}-C_6-Li^-	3.59	0.55	7.11
$2C_6$-Li	0.09	0.75	6.59	2(C_{16}-Li)	0.71	0.13	7.92
$2C_6$-Li^+	0.00	2.78	6.29	2(C_{16}-Li^+)	0.01	0.65	7.05
$2C_6$-Li^-	0.71	0.83	6.88	2(C_{16}-Li^-)	1.76	0.98	7.90
2(C_6-Li)	0.11	0.79	6.17	$2C_{24}$-Li	0.61	0.69	7.74
2(C_6-Li^+)	0.00	2.58	5.63	$2C_{24}$-Li^+	0.07	2.61	7.81
2(C_6-Li^-)	0.16	2.15	6.41	$2C_{24}$-Li^-	3.62	0.42	7.79

Table 4b. Ionization potential (IP), electron affinity (EA) and stability of different lithium-carbide clusters.

Clusters	IP (eV)	EA (eV)	Stability of neutral cluster (eV)	Stability of cationic cluster (eV)	Stability of anionic cluster (eV)
C_6-Li	8.16	–1.49	NA	NA	NA
C_6-Li^+	NA	NA	NA	NA	NA
C_6-Li^-	NA	NA	NA	NA	NA
C_6-2Li	7.17	–0.52	–5796.03	NA	NA
C_6-2Li^+	NA	NA	NA	–5813.23	NA
C_6-2Li^-	NA	NA	NA	NA	–5798.45
$2C_6$-Li	7.96	–2.95	5796.22	NA	NA
$2C_6$-Li^+	NA	NA	NA	5811.17	NA
$2C_6$-Li^-	NA	NA	NA	NA	5812.74
2(C_6-Li)	7.93	–3.47	–6008.90	NA	NA
2(C_6-Li^+)	NA	NA	NA	–6012.56	NA
2(C_6-Li^-)	NA	NA	NA	NA	–6013.28
$3C_6$-2Li	7.16	–4.44	4345.25	NA	NA
$3C_6$-2Li^+	NA	NA	NA	4351.38	NA
$3C_6$-2Li^-	NA	NA	NA	NA	4356.83
C_{14}-C_6-Li	6.90	–2.96	–10 563.97	NA	NA
C_{14}-C_6-Li^+	NA	NA	NA	–10 572.52	NA
C_{14}-C_6-Li^-	NA	NA	NA	NA	–10 584.37
2(C_{16}-Li)	5.35	–0.26	12 226.62	NA	NA
2(C_{16}-Li^+)	NA	NA	NA	12 220.36	NA
2(C_{16}-Li^-)	NA	NA	NA	NA	12 243.39
$2C_{24}$-Li	4.23	–0.74	NA	NA	NA
$2C_{24}$-Li^+	NA	NA	NA	NA	NA
$2C_{24}$-Li^+	NA	NA	NA	NA	NA

4 Conclusions

Ab initio electronic structure calculations of the lithium-carbide system have been undertaken in the present work with spin polarized generalized gradient approximation (GGA). As the first step of calculation different model structures based on standard benzene groups with Li^+ have been optimized using two different basis sets. Validity of the model structures have been checked by calculating different thermodynamic parameters. In the next stage different lithium intercalated graphite clusters based on the model structures have been optimized. Based on the optimized structure of the small clusters, bigger structures has been made and studied both in neutral as well as ionized states. Finally, different physical parameters of the structures, i.e., dipole moment, ionization potential, electron affinity and binding energy have been calculated. It is found that these properties vary with the ionization states of the cluster. To get an idea about the charge distribution in different orbitals, HOMO and LUMOs of each cluster have been calculated and discussed under ground state of different structures. The reality and the acceptance of the structures have been checked by studying infrared and Raman spectrum of the optimized small and medium model clusters only. Stability graphs of the lithium graphite show that clusters with total number of atoms 13, 20 and 33 are always magic in nature. Variation of binding energy shows that the binding energy in the clusters increases with increasing number of atoms. However in the case of medium size clusters, the binding energies are relatively low. In each group of cluster there is no variation of stabilities, but between different groups, there is a wide difference. Variation of HOMO-LUMO gap, charge on the Li atom, chemical potential and hardness and their ratio with the number of atoms in the cluster show that the smaller, symmetric and the relatively bigger clusters are better as charge conductors than the medium size clusters. Therefore, when small symmetric clusters form bigger clusters with wide separation between the lithium atoms in between the graphite plane, the medium behaves as a better conducting medium as well as showing high charge storage capacity.

References

1. C. Julien, G.A. Nazri, *Solid State Batteries: Materials Design and Optimization* (Kluwer Academic Publishers, Norwell, MA, 1994)
2. A.R. Armstrong, P.G. Bruce, Nature **381**, 499 (1996)
3. M. Brousselya, P. Biensan, B. Simon, Electrochimica Acta **45**, 3 (1999)
4. W.R. McKinnon, R.R. Haering, in *Modern Aspects of Electrochemistry*, edited by B. Conway, R.E. White, J. O'Mara Bockris (Plenum Press, New York, 1983), Vol. 15, p. 235
5. D.P. Wilkinson, J.R. Dahn, U. von Sacken, D.T. Fouchard, *The Electrochemical Society Extended Abstracts* (Seattle, Washington, USA, 1990), Vol. 90, pp. 85–87
6. U. von Sacken, J.R. Dahn, Electrochimica Acta **45**, 121 (1999)
7. J.R. Dahn, R. Fong, M.J. Spoon, Phys. Rev. B **42**, 6424 (1990)
8. J.R. Dahn, Phys. Rev. B **44**, 9170 (1991)
9. K.R. Kganyago, P.E. Ngoepe, C.R.A. Catlow, Solid State Ionics **159**, 21 (2003)
10. N. Chakraborti, R. Jayakanth, S. Das, E.D. Çalişir, Ş. Erkoç, J. Phase Equilib. Diffus. **28**, 140 (2007)
11. K. Nishidate, K. Sasaki, Y. Oikawa, M. Babu, M. Hasegawa, Surf. Sci. Nanotech. **3**, 385 (2005)
12. K. Burke, J.P. Perdew, Y. Wang, in *Electronic Density Functional Theory: Recent Progress and New Directions*, edited by J.F. Dobson, G. Vignale, M.P. Das (Plenum, 1998)
13. J.P. Perdew, in *Electronic Structure of Solids '91*, edited by P. Ziesche, H. Eschrig (Akademie Verlag, Berlin, 1991)
14. J.P. Perdew, J.A. Chevary, S.H. Vosko, K.A. Jakson, M.R. Pederson, D.J. Singh, C. Fiolhais, Phys. Rev. B **46**, 6671 (1992)
15. J.P. Perdew, J.A. Chevary, S.H. Vosko, K.A. Jakson, M.R. Pederson, D.J. Singh, C. Fiolhais, Phys. Rev. B **48**, 4978 (1993)
16. J.P. Perdew, K. Burke, Y. Wang, Phys. Rev. B **54**, 16533 (1996)
17. J. Wang, J.G. Han, J. Chem. Phys. **123**, 064306 (2005)
18. J.G. Han, F. Hagelberg, J. Mol. Struct. Theochem **549**, 165 (2001)
19. P. Guo, Z.Y. Ren, F. Wang, J. Bian, J.G. Han, G.H. Wang, J. Chem. Phys. **121**, 12265 (2004)
20. L.J. Guo, X. Liu, G.F. Zhaoa, Y.H. Luo, J. Chem. Phys. **126**, 234704 (2007)
21. M.J. Frisch, G.W. Trucks, H.B. Schlegel, G.E. Scuseria, M.A. Robb, J.R. Cheeseman, V.G. Zakrzewski, J.A. Montgomery Jr, R.E. Stratmann, J.C. Burant, S. Dapprich, J.M. Millam, A.D. Daniels, K.N. Kudin, M.C. Strain, O. Farkas, J. Tomasi, V. Barone, M. Cossi, R. Cammi, B. Mennucci, C. Pomelli, C. Adamo, S. Clifford, J. Ochterski, G.A. Petersson, P.Y. Ayala, Q. Cui, K. Morokuma, D.K. Malick, A.D. Rabuck, K. Raghavachari, J.B. Foresman, J. Cioslowski, J.V. Ortiz, A.G. Baboul, B.B. Stefanov, G. Liu, A. Liashenko, P. Piskorz, I. Komaromi, R. Gomperts, R.L. Martin, D.J. Fox, T. Keith, M.A. Al-Laham, C.Y. Peng, A. Nanayakkara, M. Challacombe, P.M.W. Gill, B. Johnson, W. Chen, M.W. Wong, J.L. Andres, C. Gonzalez, M. Head-Gordon, E.S. Replogle, J.A. Pople, *Gaussian 98, Revision A.9* (Gaussian Inc., Pittsburgh PA, 1998)
22. L.G. Scanlon, D.M. Storch, J.H. Newton, G. Sandi, *Energy Conservation Engineering Conference, IEEE-97, Proceedings of the 32nd Intersociety* (1997), Vol. 1, pp. 87–92
23. R.G. Parr, W. Yang, *Density-Functional Theory of Atoms and Molecules* (Oxford Science Publications, New York, 1989), pp. 91–92